FRAGMENTATION EVENT MODEL AND ASSESSMENT TOOL (FREMAT) SUPPORTING ON-ORBIT FRAGMENTATION ANALYSIS

Roxana Larisa Andrișan [(1)], Alina Georgia Ioniță [(1)], Raúl Domínguez González [(2)], Noelia Sánchez Ortiz [(2)], Fernando Pina Caballero [(1)], Holger Krag [(3)]

[(1)] Deimos Space S.R.L. , Strada Buzesti 75-77, sector 1, 011013,Bucuresti, Romania, Email: roxana-larisa.andrisan@deimos-space.com
[(2)] Deimos Space, Ronda de Poniente 19, 28760, Tres Cantos, Madrid, 28760, Spain, Email: noelia.sanchez@deimos-space.com
[(3)] ESA/ESOC Space Debris Office (OPS-GR), Robert-Bosch-Str. 5, 64293 Darmstadt, Germany, Email: holger.krag@esa.int

ABSTRACT

The Fragmentation Event Model and Assessment Tool (FREMAT) project for ESA was completed with the objectives of simulating on-orbit fragmentations, assessing their impact on the space population and evaluating the capability of identification of fragmentation events from existing surveillance networks. In the frame of the FREMAT activity, the implementation of several algorithms related to on-orbit fragmentation events was carried out. FREMAT encompasses three individual tools: Fragmentation Event Generator (FREG), Impact of Fragmentation Events on Spatial density Tool (IFEST) and SOFT (Simulation of On-Orbit Fragmentation Tool).

Fragmentation Event Generator (FREG) has been conceived to simulate fragmentation events (explosion and collisions). A breakup model based on recent approaches was the baseline for this tool .We have enhanced the baseline NASA break up model, in order to ensure the consistency of mass and momentum in the created fragment clouds.

The second tool, IFEST, allows the evaluation of the impact of on-orbit fragmentations in the space debris population. This tool employs a fast semianalytic propagator for computing the long-term evolution of the clouds of fragments (up to hundreds of years) obtained from FREG, and computes the spatial density caused by those fragments as well as the percent increase in the background spatial density obtained from MASTER.

Finally, the third tool, SOFT, has been created to simulate the determination of the type of fragmentation and the objects involved in a fragmentation event when a space surveillance network detects a number of unexpected new objects and a fragmentation event is considered a possible cause. The tool determines the type of fragmentation computes the time and location of the event and identifies the parent objects.

This paper presents a description of the algorithms implemented in this toolkit and a brief summary of their main functionalities. Furthermore, results from simulations of passed fragmentation events are reported. Short and long-term evolutions of the clouds are analysed, as well as the feasibility of determining the location and time of the fragmentation event.

1 DESCRIPTION OF THE TOOLS

The objectives of FREMAT cover three different aspects: improvement of the algorithms and methods to be used for issues related to fragmentation events; software implementation to apply those algorithms; and analysis to derive conclusions on the fragmentation problem in regard to the impact on Space population and Space Surveillance Systems.

1.1 Fragmentation Event Generator (FREG)

The Fragmentation Event Generator (FREG) has been created to simulate the generation of space debris as an outcome from fragmentation event (explosion and hypervelocity collisions). The key to provide good short- and long-term debris impact risk assessments is the ability to reliably predict the outcome of a satellite breakup. A commonly used model to describe the product of satellite fragmentation is the NASA standard breakup model which has been updated several times for the ESA MASTER tool. The MASTER 2009 NASA Breakup Model was employed in order to implement this tool (refer to [2]). It is a statistical model found based on space surveillance data and a few ground-based test data. The model takes the mass, impact velocity magnitude for input and provides the fragment size, area-to-mass ratio, velocity magnitude distributions for output.

Although the design and development of the algorithm are based on the equations presented in the MASTER Final Report [2] additional mathematical and statistical functions are needed for the implementation of those expressions. Furthermore, physical and mathematical constraints are added to the fundaments of the

fragmentation model, which increases the complexity of the algorithm.

- Area-to-mass ratio distributions

The MASTER 2009 NASA Breakup uses two bi-modal normal distribution to assign an area-to-mass ratio to generated large fragments (one for spacecraft and one for rocket bodies) and a simple normal distribution (small fragments distribution).

For rocket body breakups, the distribution function is used for fragments larger than 11 cm, while the small fragment distribution function is used for fragments smaller than 1.7 cm. A similar distinction is made for spacecraft breakups, so that the spacecraft distribution function is used for fragments larger than 11 cm and the small fragment distribution function for fragments smaller than 8 cm. An additional function is used to bridge the gap in between 1.7 and 11 cm for rocket bodies and between 8 and 11 cm for spacecraft. A summary of all used distributions is shown in Tab.1. The principal normal distributions and their parameters are defined in [2], as well as the formula for average cross-sectional area as a function of dimeter and the formula that computes the mass of the fragments.

Table 1: Area-to-mass Distribution Functions

	d ≤ 1.7 cm	**1.7 < d < 11 cm**	**d ≥11**
Rocket bodies	Small fragments distribution	Bridging function	Rocket bodies distribution (bi-modal)
	d ≤ 8 cm	**8 < d < 11 cm**	**d ≥11**
Spacecraft	Small fragments distribution	Bridging function	Spacecraft distribution (bi-modal)

- Size distribution

In the MASTER 2009 NASA Breakup Model, the cumulative number of fragments derived from a fragmentation event is described by means of a single power law distribution for both collision and explosions.

The number of fragments distribution versus size is then given as:

$$N_f(d) = \begin{cases} 6s\hat{d}^{-1.6} & for\ explosions \\ 0.1\hat{m}_e{}^{0.75}\hat{d}^{-1.71} & for\ collisions \end{cases} \quad (1)$$

where the normalised ejecta mass $\hat{m}_e = \frac{m_e}{kg}$ is governed by

$$\hat{m}_e = \begin{cases} \frac{m_{sat} + m_p}{1\ kg} & \forall \hat{E}_p \geq \hat{E}_p{}^* \\ \frac{m_p v_i}{1000 \frac{kgm}{s}} & \forall \hat{E}_p < \hat{E}_p{}^* \end{cases} \quad (2)$$

- $d =$ fragment diameter $[m]$
- $\hat{d} = \frac{d}{1\ m}$ (normalised fragment diameter)
- $N_f =$ cumulative number of fragments $> d$
- $v_i =$ impact velocity $[m/s]$
- $m_p =$ projectile mass $[kg]$
- $m_{sat} =$ parent object mass $[kg]$
- $s =$ scaling factor
- $\hat{E}_p = \frac{m_p}{2m_{sat}} v_i^2$ (specific kinetic energy of projectile [J/g])
- $\hat{E}_p{}^* = 40\ J/g$ (critical specific energy)

For future fragmentations, NASA model assumes some standard values for the scaling factor (refer to [2] for those values). For historical events, the scaling factor is derived from the number of catalogued fragments.

The branch of Eq.1 devoted to explosions is used unchanged for the present implementation.

Since N_f does not depend on the mass of the parent object, the scaling factor (s) is the only parameter that can change the cumulative number of fragments for each characteristic length. Hence, mass consistency cannot be ensured by an adequate choice of model parameters. Therefore, the algorithm generating the particles has to track the consumed mass.

The strategy adopted in FREG, in order to fulfil mass consistency, is to reject the most massive fragments until we conserve or accumulate less than the initial total mass. If, after discarding those fragments, the total mass is lower than the mass of the parent object, an additional fragment whose mass matches exactly the difference between the total mass and the initial mass is added.

In case of collisions, as shown in Eq. 1 a new variable is involved, the ejecta mass. The ejecta mass depends on the specific kinetic energy, which defines whether the collision is catastrophic or non-catastrophic (if the kinetic energy is greater than the critical kinetic energy the collision is catastrophic). Furthermore, in this case, two parent objects are involved instead of one. In spite of the fact that two colliding objects are taken into account, Eq. 1 does not make a distinction as to which fragments belong to each object. Therefore, a unique cloud of objects obtained from both objects is assumed in the NASA breakup model.

In FREG, Eq. 1 and Eq. 2 are slightly modified in order to get two differentiate clouds, one for each object, even one of the clouds could contain a very small number of fragments or only one object. For the sake of this purpose, collisions are separated in two fictitious sub-collisions. Hence, if the colliding objects are called collidingObject1 and collidingObject2, the first sub-collisions is defined in such a way that collidingObject1 is assumed to be the target and collidingObject2 is assumed to be the projectile. For the second sub-collision, the roles of the colliding objects are inverted. Thus, the first sub-collisions will define the fragmentation of collidingObject1 and the second sub-collisions will define the fragmentation of collidingObject2.

The ejecta mass for each sub-collision must be defined based on Eq. 4 taking into account the impact velocity is the same for both sub-collisions and equal to the relative velocity between the colliding objects in the original collision:

First sub-collision:

$$\hat{m}_{e_1} = \begin{cases} \dfrac{m_{\text{collidingObject1}}}{1\ kg} & \forall \hat{E}_{p_1} \geq \hat{E}_p{}^* \\ \dfrac{m_{\text{collidingObject2}} v_i}{1000 \dfrac{kgm}{s}} & \forall \hat{E}_{p_1} < \hat{E}_p{}^* \end{cases} \quad (3)$$

$$\hat{E}_{p_1} = \frac{m_{\text{collidingObject2}}}{2\, m_{\text{collidingObject1}}} v_i^2 \quad (4)$$

Second sub-collision:

$$\hat{m}_{e_2} = \begin{cases} \dfrac{m_{\text{collidingObject2}}}{1\ kg} & \forall \hat{E}_{p_2} \geq \hat{E}_p{}^* \\ \dfrac{m_{\text{collidingObject1}} v_i}{1000 \dfrac{kgm}{s}} & \forall \hat{E}_{p_2} < \hat{E}_p{}^* \end{cases} \quad (5)$$

$$\hat{E}_{p_2} = \frac{m_{\text{CollidingObject1}}}{2\, m_{\text{CollidingObject2}}} v_i^2 \quad (6)$$

When the ejecta mass is computed, Eq. 1 is used for the computation of the cumulative number of fragments for each colliding object. Once the cumulative number of fragments is obtained for each colliding object (CNF1 and CNF2), the process employed for the computation of the differential number of fragments (NF1 and NF2) and for the application of the conservation of mass is the same as the one used for explosions. The only difference is that in this case the procedure for each colliding object must be applied.

- Velocity distribution

For the additional velocities acquired by the fragments the model employs a normal distribution, as stated in [2].

The model does not reveal the directions of the additional velocities imparted.

In FREG, conservation of momentum is used to determine fragment direction. Following physical laws, both collision and explosions satisfy the conservation of lineal momentum.

The technique adopted in the present model for this purpose is based on distributing the delta-velocities vectors uniformly around the centre of mass of each parent object (from collisions or explosions).

Another physical aspect that must be taken into account, in this case only for collisions, is the conservation of kinetic energy. However, the energy is not exactly conserved since a hypervelocity impact is not an ideal elastic collision; part of the energy is dissipated during impact.

Oftentimes the cumulative kinetic energy of the fragments after mass and momentum conservation is less than the total initial energy of the colliding objects.

For the present model, the quantity of dissipated energy is not determined. Therefore, once the conservation of momentum and mass consistency are applied, if the total energy is greater than the initial energy, then all additional velocities are scaled downward until energy is conserved, assuming the loss energy is null. On the other hand, if the total energy is lower than the initial energy, the difference is assumed to be the loss energy and no scaling actions are applied.

- Inputs and outputs

The user must specify the following inputs for the tool:

- Type of event (explosion/collision)
- Type of object (spacecraft/ rocket body)
- Mass of the parent(s) object(s)
- State vector(s) of the parent object(s) at event epoch
- Scaling factor (for explosion)

FREG also requires a discretization as input for the computation of representative fragments. For each characteristic length (diameter), the fragmentation model yields a number of fragments, a value for delta-velocity and an area-to-mass ratio. For each fragment, a direction for the additional velocity is computed strategically in order to follow the conservation of momentum. Therefore, each group of fragments with identical size obtained from the fragmentation model will contain a number of fragments with different directions of additional velocity vectors, but with the same magnitude. Hence, a discretization of orbital

elements for each characteristic length is needed in order to categorise different representative orbits. Additionally, a discretization of characteristic length is introduced with the intention of classifying the complete cloud in representative fragments. Once the discretization is defined, by specifying maximum and minimum values of the range and the number of intervals for each parameter (orbital elements and size), FREG is able to count and classify similar orbits and use the average of the parameters of every group of similar fragments to define a new representative fragment. The discretization is linear for all orbital elements and for size. S. Additionally, the user can enable a logarithmical discretization for size, semi-major axis and eccentricity.

As outputs, the tool provides: one or two (depending on the event type) files containing one or two clouds of representative fragments, auxiliary files with additional information of the generated fragments and scripts for plotting. Some examples of the outcomes are presented in the following sections.

1.2 Fragmentation Events on Spatial density Tool (IFEST)

The Impact of Fragmentation Events on Spatial Density Tool (IFEST) allows long-term propagation of fragments obtained in a fragmentation event by means of a DSST semianalytic propagator. The tool uses the main output files generated with FREG as inputs for the propagation.

Long-term evaluation of the evolution of the clouds generated by a fragmentation event requires fast propagators that allow adequately accurate propagations of large numbers of objects. Semianalytical techniques were chosen to be used in IFEST since they are the most suitable for the objective of the tool in terms of run-time performance and required propagation accuracy.

The Draper Semianalytic Satellite Theory (DSST) propagator (refer to [1] for more details) isused as implemented in Orekit. Orekit is a space dynamics library written in Java. It aims at providing accurate and efficient low level components for the development of flight dynamics applications. It is designed to be easily used in very different contexts, from quick studies to critical operations. Version 7.0 of Orekit library from [5] is employed in IFEST.

IFEST also computes spatial density as a function of altitude and/or longitude for each propagation time step.

The debris environment of the Earth can be characterised using the concept of spatial density computed within the volume of a spherical shell, which has dimensions of geocentric radius (altitude).

Spatial density as a function of altitude is calculated by filtering out the objects passing through a spherical geocentric shell at a specific epoch. Then, the number of fragments obtained is divided by the volume of the spherical shell computed as exposed in Eq.7.

$$V_{shell} = \frac{4}{3}\pi(R^3 - r^3) \quad (7)$$

- R is the outer radius of the shell [km]
- r is the inner radius of the shell [km]
- V_{shell} is the volume of the shell in [km^3]

Hence, the spatial density as a function of altitude fulfils:

$$SD_{altitude} = NF_{shell}/V_{shell} \quad (8)$$

- $SD_{altitude}$ is the spatial density as a function of altitude [NF/km^3].
- NF_{shell} is the number of fragments within the spherical shell at a specific epoch.

Then, the value of the spatial density is assigned to the midpoint of the interval$(\Delta r/2)$.

For each spherical shell, spatial density as a function of geocentric longitude (Eq. 9) can be computed. In the present document, this function is calculated by dividing the spherical shell in several equidistant cells. The value of the spatial density is assigned to the midpoint of the arc $\Delta\lambda/2$.

$$SD_{longitude} = NF_{longitude}/V_{shell} \quad (9)$$

- $SD_{longitude}$ is the spatial density as a function of longitude within a specific spherical shell
- $NF_{longitude}$ is the number of fragments within a longitudinal cell

The fragmentation clouds are fed directly from FREG. IFEST also allows: defining the size of shells for spatial density computation (altitude-based spatial density, also longitude-based), defining the DSST Propagator configuration (number of zonals/tesserals, Solar radiation pressure (SRP) and drag perturbation enabled/disabled), setting the duration and output step for the analysis (propagation and computation of spatial density) and optionally running ESA MASTER tool automatically from IFEST, for comparison purposes. This last capability allows obtaining the percent increases in background spatial density and assessing the impact of the fragmentation event on the existing space population.

A sample population cloud and the spatial density generated with POEM-2005 were provided by ESA in order to validate the spatial density computed with IFEST.

The cloud was propagated one full revolution and the spatial density was obtained for each time step as a function of altitude. Then, an average value of spatial

density was computed in order to obtain an overall value of spatial density for one full revolution as a function of altitude.

Fig. 1 illustrates that the spatial densities are almost coincident, except for spiky structure that are likely to be caused by the number of intervals of time (number of time steps of propagations) used for the computation of the average spatial density.

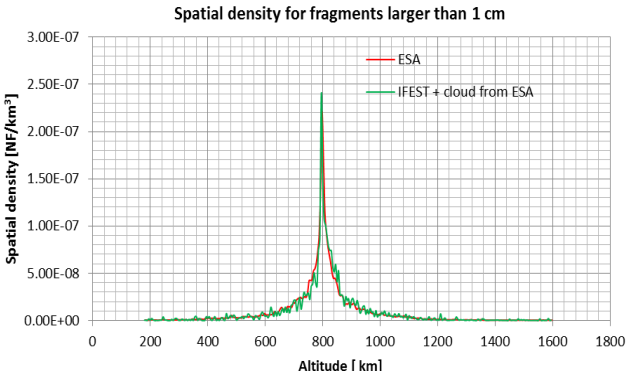

Figure 1: Comparison of spatial densities using the cloud provide by ESA

1.3 Simulation of On-Orbit Fragmentation Tool (SOFT)

A possible fragmentation can be envisaged when several new objects are detected and they cannot be correlated with any object in the catalogue and they cannot be identified as a result of a launch event or correlated to a manoeuvre of a known object. SOFT was created to determine the type of fragmentation (explosion or collision), the time and place of the event and the objects involved in it (called "parents" in this document).

The first step is to identify the type of fragmentation. Using a cloud of fragments (detected as new objects) the algorithm has to establish if the event was an explosion or a collision. For this purpose the classical orbital elements of the fragments included in the cloud are analysed in order to determine whether they follow a bimodal distribution or not. If there are large differences between the classical orbital elements of the fragments (i.e. a bimodal distribution was detected for one or more orbital elements) then it can be assumed the event was a collision, otherwise it was an explosion.

The input for the fragmentation event identification tool is only one cloud containing all the fragments released in the event. If the type of fragmentation after the execution of the step described in the previous section is concluded to be an explosion, then all fragments must belong to only one cloud and no separation of the clouds is needed. If the type of fragmentation is estimated to be a collision, the initial cloud of fragments must be divided in two separate sub-clouds, one for each colliding object (i.e. for each parent object).

The strategy adopted in this module for grouping the fragments in case of collision is based on the previous mentioned bimodal distributions, as the dispersion of the orbital elements of the fragments is assumed to be respecting this type of distribution in case of collision.

In case all fragments are on non-equatorial orbits, the main orbital elements used are inclination, right ascension of the ascending node (RAAN) and radius of perigee and apogee. Four methods were created for the allocation of the fragments to the corresponding cloud, depending on the difference between the minimum and maximum values for inclination and RAAN inside the cloud.

In case that, inside the cloud, there are fragments on equatorial orbits, the main orbital elements used are inclination, eccentricity and radius at perigee and apogee. Three methods were created for the allocation of the fragments to the corresponding cloud, depending on the difference between the minimum and maximum values for inclination and eccentricity inside the cloud.

Once the fragments are distributed to the corresponding cloud, the two fragmentation clouds are analysed separately.

The method used in the SOFT tool to identify the fragmentation event relies on backward propagation of the objects within the cloud in order to allow the computation of the average distance of the fragments to the centre of mass of the cloud for each propagation step. The position of the centre of mass and time corresponding to the minimum average distance are considered to be the position and, respectively, the time of the event. For a precise determination of the event, the model uses a numerical propagator for the backward propagation.

- Finding position and time of the event

The position and time of the event are identified with the help of the centre of mass. In each time step of backward propagation the position of the centre of mass is computed using:

$$\vec{R} = \frac{1}{M}\sum_{i=1}^{n} m_i \vec{r}_i \qquad (10)$$

For Eq. 10 it is considered a cloud of objects P_i , $i = 1, \dots, n$ each with mass m_i that are located in space by position vectors $\vec{r}_i, i = 1, \dots, n$ and M is the sum of the masses of all of the objects. $\vec{R}$ is the position vector of the centre of mass.

For each time step of backwards propagation, the model computes the distance between each fragment and the position of the centre of mass, as well as the average of

these distances. If the value of the average distance is smaller than a threshold imposed in the model (50 km), the time step is reduced and the backwards propagation continues until a minimum value is found.

The velocity of the parent objects involved in a fragmentation event (each colliding object or the exploding object) at the moment of the event can be computed by means of Eq. 11, where i is the total number of fragments generated in the fragmentation event coming from each of the fragmented objects. This equations result from the conservation of momentum.

$$\vec{V}_{parent} = \frac{\sum_i m_i \left(\vec{V}_i\right)}{\sum_i m_i} \tag{11}$$

- $\vec{V}_{parent}$ is the velocity vector of one of the parents
- $\vec{V}_i$ is the velocity vector of fragment i coming from its $parent$ immediately before the fragmentation event.
- m_i is the mass of fragment i coming from its $parent$ immediately before the fragmentation event.

- Comparison with background catalogue

The true objects involved in the fragmentation are determined by comparing the computed orbit with the background catalogue. SOFT tool requires two input catalogues, one for the background population, and another one containing the fragments.

For a precise comparison with the background catalogue, only the objects inside the pre-event catalogue that are likely to be near the position of the event at the time of the breakup are selected and propagated to the time of event identified. In case the event occurred on an equatorial orbit, then the comparison uses radius of perigee and apogee as criteria, otherwise inclination and RAAN are used. All the objects that are between the imposed margins from the orbits of the computed parents are considered possible candidates.

An important issue to be considered is that in a real situation, inside a cloud there could be many objects that are not related to the event. These fragments might contaminate the results and should be eliminated from the cloud. The model attempts to remove all these foreign fragments.

2 SIMULATION CASES

The purpose of this document is to show the capabilities and functionalities of the tools described in previous sections. Fragmentation event cases are simulated and evaluated. The final objective is to analyse the behaviour of the generated clouds of cases of fragmentation are simulated. Both of the simulated fragmentation events actually occurred. These are the collision between Cosmos 2251 and Iridium 33 and the explosion of the BREEZE-M Rocket body (NORAD id 41122).

The two selected cases cover distinct orbit regimes, altitudes and cloud shapes.

The collision between Cosmos 2251 and Iridium 33 is one of the most important fragmentation events of the last years. The 2009 satellite collision was the first accidental hypervelocity collision between two intact artificial satellites in low Earth orbit (LEO). For this collision, the state vector at the epoch of the collision is obtained by means of a propagation of the orbital elements exposed in ESA DISCOS database (refer to [3]). As those orbital elements do not correspond to the actual moment of collision, an intersection of the orbits of the two colliding objects must be computed in order to find the desired state vector. Thus, both objects are propagated in time and an approximate intersection point is obtained.

Regarding the second fragmentation case, on 20 January 2016, at approximately 1900 UTC, the JSpOC (Joint Space Operations Center) identified a possible breakup of a Breeze-M R/B (NORAD id 41122). The Joint Space Operations Center identified the possible breakup of the rocket stage on January 20 when at least ten pieces of debris were identified in close orbital proximity to the spent rocket body, in Geosynchronous Orbit (GEO).

The main inputs for the simulation tools (specifications, state vectors and orbital elements of both fragmentation events) are summarised in Tab. 2 and Tab.3.

A summary of the outcome obtained from the fragmentation tool for the fragmentation event is outlined in Tab. 4 and in plots from Fig.2 and Fig. 3. Fig. 2 represents the area-to-mass distribution of the fragments (larger than 1 cm) obtained with FREG for Iridium 33 (the distribution for Cosmos 2251 and Breeze-M R/B are similar and they are omitted in the present document). The two branches of the large object law and the single distribution for small particles as well as the bridging function mentioned in 1.1 are visible in this plot. Fig. 3 represents the distribution of the additional velocities of fragments (larger than 1 cm) for the collision and for the explosion. The reader can observe the majority of the points are into a confidence interval of $\pm 2\sigma$, where σ is the standard deviation of each distribution. In addition, the region close to the central line of the distribution which represents the mean value, is more congested, as expected in a statistical distribution. These figures also show that the values of additional velocities obtained by the fragments derived from the explosion reach lower values than those coming from the collision.

Table 2: Event epoch and specifications

Event type	Object type	Simulation epoch	Mass (kg)
Explosion (Scaling factor = 1.0)	Rocket Body	2016-01-19 T19:05:16.107	1600
Collision (Impact velocity = 11.625 km/s))	Spacecraft	2009-02-10 T16:56:0.000	556
	Spacecraft		900

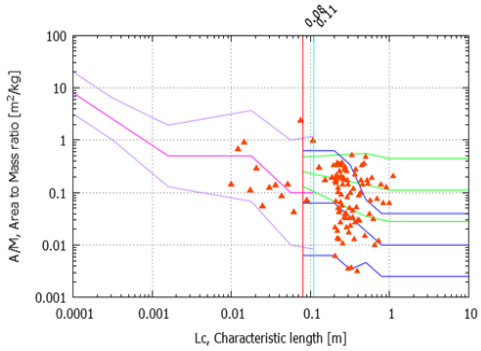

Figure 2: Mean value and ±2 σ confidence interval for the bi-modal normal distribution used for area-to-mass

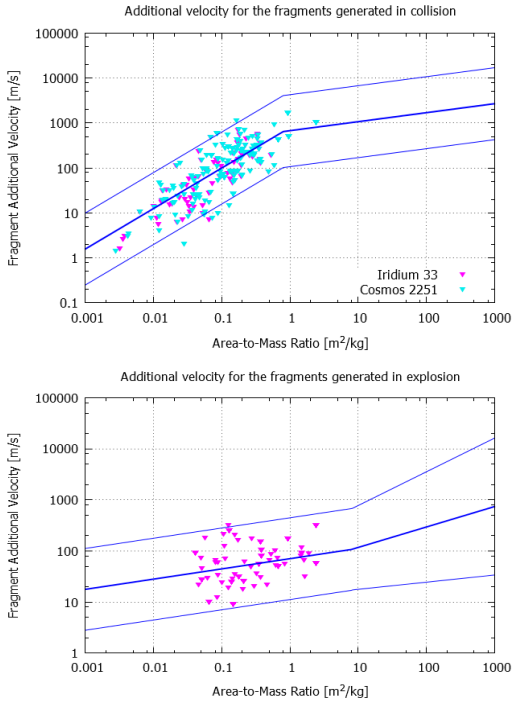

Figure 3: Delta-V vs. A-to-M of fragments for Cosmos-Iridium (top), Breeze-m R/M (bottom) (mean value and ±2 σ of the distribution

Table 3: State vectors and orbital elements at the event epoch

		State vector at the simulation epoch (reference frame : inertial EME2000)					
Event type	**Parent object**	**X [km]**	**Y [km]**	**Z [km]**	**Vx [km/s]**	**Vy [km/s]**	**Vz [km/s]**
Explosion	Breeze-M R/B	40232.08	-12671.15	-1489.24	0.87748	2.89889	-0.00882
Collision	Iridium 33	-1358.44	1396.74	6878.69	3.63364	-6.21411	1.97441
	Cosmos 2251				-7.01143	-2.42651	-0.82963

		Orbital elements at the simulation epoch (reference frame : inertial EME2000)					
Event type	**Parent object**	**SMA [km]**	**Ecc**	**Inc [deg]**	**RAAN [deg]**	**AOP [deg]**	**M [deg]**
Explosion	Breeze-M R/B	41031.95	0.03069	2.0309	77.8684	64.13039	201.7828
Collision	Iridium 33	7144.58	0.00092	86.3834	121.3099	210.5347	224.1327
	Cosmos 2251	7147.09	0.00804	75.8037	17.4687	4.36715	91.7549

Table 4: Summary results from FREG

Type of event	Num. of fragments > 1 cm	Num. of fragments > 10 cm	Total num. of fragments	Num. of representative fragments
Breeze-M R/B	11056	248	23886430232	136 (> 10 cm) and 595 (>1 cm)
Iridium 33	35378	608	208356039523	484 (>1cm)
Cosmos 2251	50773	876	299007362445	876 (>1cm)

2.1 Collision between Cosmos 2251 and Iridium 33

Fig. 4 presents the Gabbard diagram immediately after the fragmentation event. This plot represents the perigee and apogee altitudes of the fragments versus the semi-major axis and the plotting script for creating them is automatically generated in IFEST. As illustrated in the Gabbard diagram, many of the generated fragments concentrate around the altitude of the collision (790.966 km) after the breakup.

The fragments achieve additional velocities during the collision, which leads to the variation of the orbital elements of the parent object, obtaining a new orbit for each fragment immediately after the explosion. For small additional velocities the slight variation of the orbital elements lead to similar altitudes for perigee and apogee, as the orbit of the parent object is near-circular. For larger additional velocities, the orbits of the fragments tend to separate from the parent object orbit. Thus, the variation of the eccentricity yields different altitudes for perigee and apogee.

The Gabbard diagram shows the characteristic X-shape, with the top part representing the apogees, and the bottom part showing the perigees. Objects near the crossing point received no along-track delta-velocity (hence no change in semi-major axis).Objects left of the crossing point maintained their apogees and lowered their perigees due to negative along-track delta-velocity and objects towards the right maintained their perigees and raised their apogees due to positive along-track delta-velocity.

Fig. 5 represents the Gabbard diagram provided by ESA for the collision between Cosmos and Iridium. If a comparison is made between these two figures, it is visible that the shapes of the plots are very similar.

The cloud of fragments obtained from FREG for the Cosmos 2251-Iridium 33 collision are fed into IFEST and propagated in time. Fig. 6 shows that the fragments disperse in the along-track direction quickly since the periods of the orbits are quite smaller than one day and the fragments complete several orbital revolutions after 1 day. The effect of perturbations produced by drag and the oblateness of the Earth (J2), as well as the additional

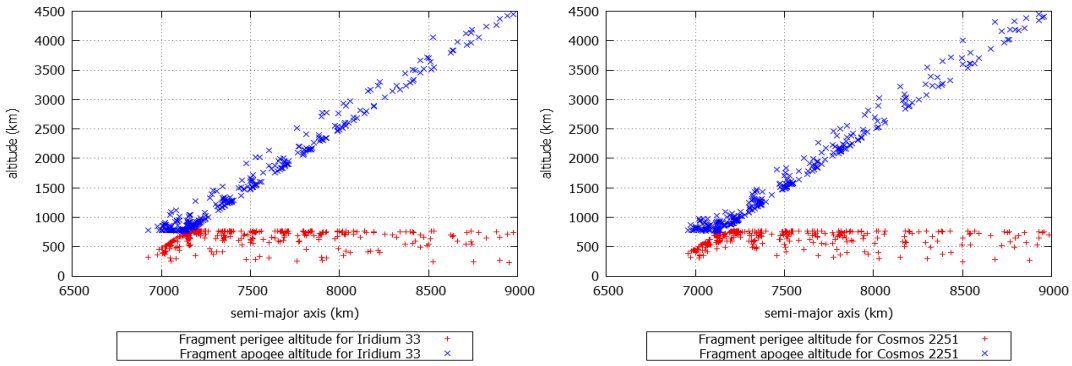

Figure 4: Gabbard diagrams from FREG for collision at the event epoch, left plot corresponds to the Iridium 33 fragments, whereas right plot is associated to the Cosmos 2251 pieces

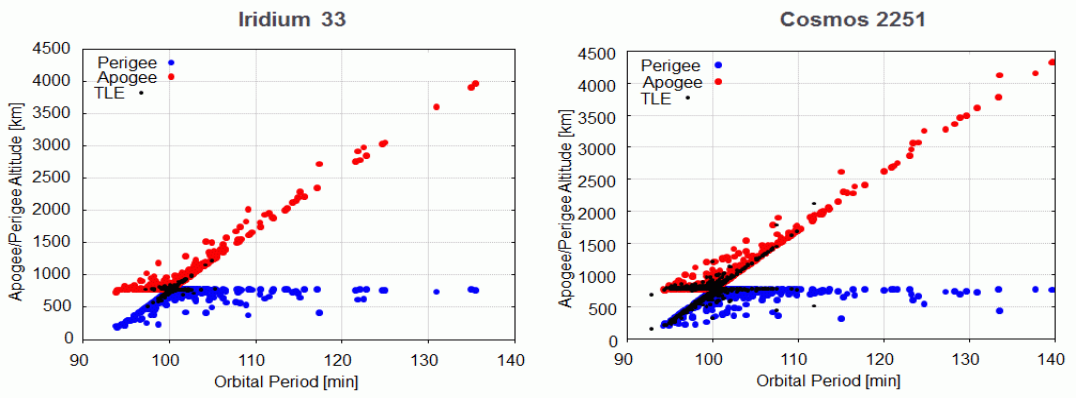

Figure 5: Gabbard diagram for the collision between Cosmos 2251 and Iridium 33 (provided by ESA)

velocities gained by the fragments during the collision make possible the cross-track dispersion. Debris objects from both colliding objects form a spherical shell around the geoid and some of the fragments also re-enter due to the effect of drag. After one hundred years, only a few fragments remain in orbit. Nevertheless, during the first years, the fragments represent a hazard for the LEO protected region. IFEST also computes the

spatial density as a function of altitude. The computation is completed for different propagation duration and time steps as shown in Fig. 7 and Fig. 8. Some periodic patterns are visible, which could be a consequence of the periodicity of perturbations. All the following plots devoted to spatial density for Cosmos/Iridium collisions show an initial crowded altitude (the altitude of collision marked in green). The fragments tend to move to lower altitudes over time until they re-enter. Additionally, the altitude range covered by the cloud seems to be almost constant along time except for the case where most of the objects tend to re-enter.

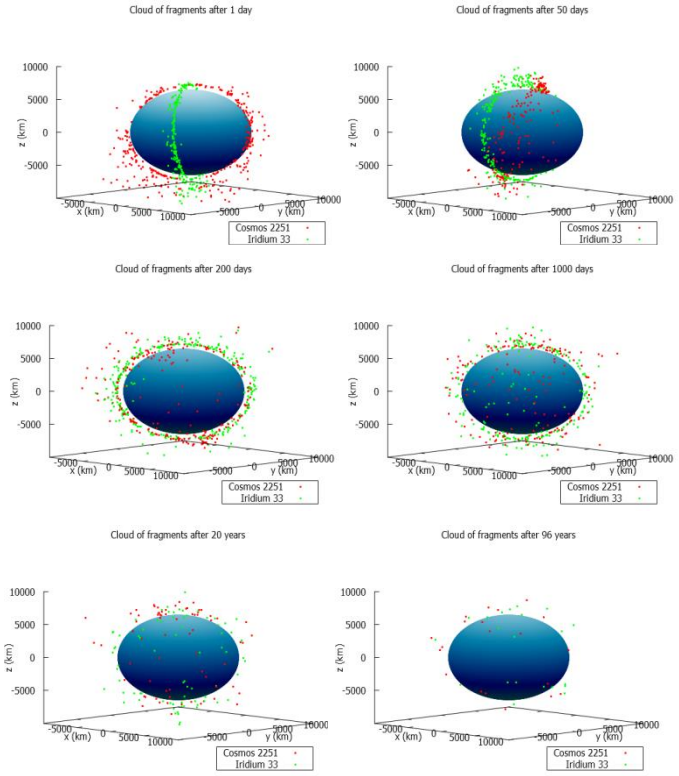

Figure 6: Evolution of the fragmentation clouds from Cosmos 2251-Iridium 33 collision. From left to right and from top to bottom, the : 1 day, 50 days, 200 days, 1000 days, 20 years and 96 years.

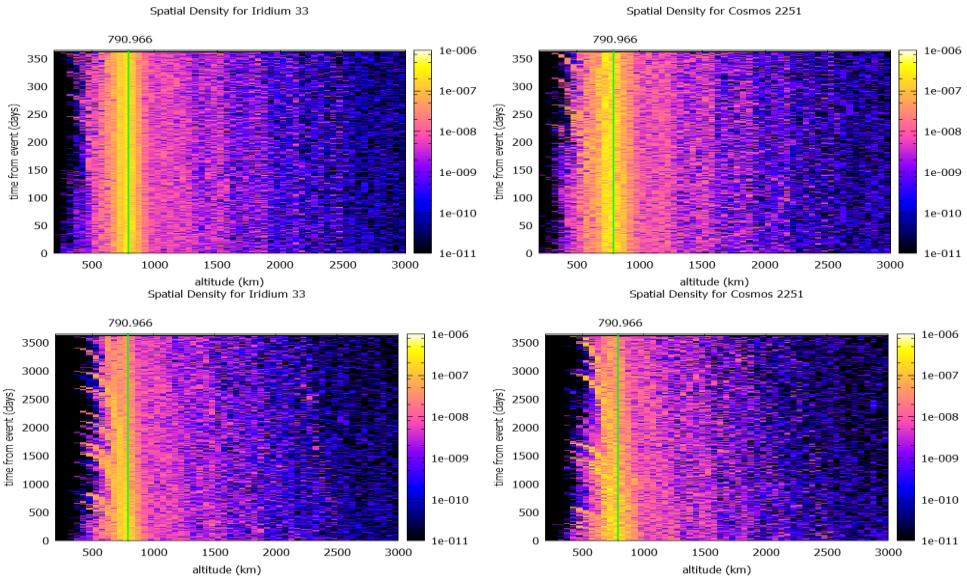

Figure 7: Spatial density for Cosmos-Iridium as a function of altitude over 1 year (top) and over 10 years (bottom)

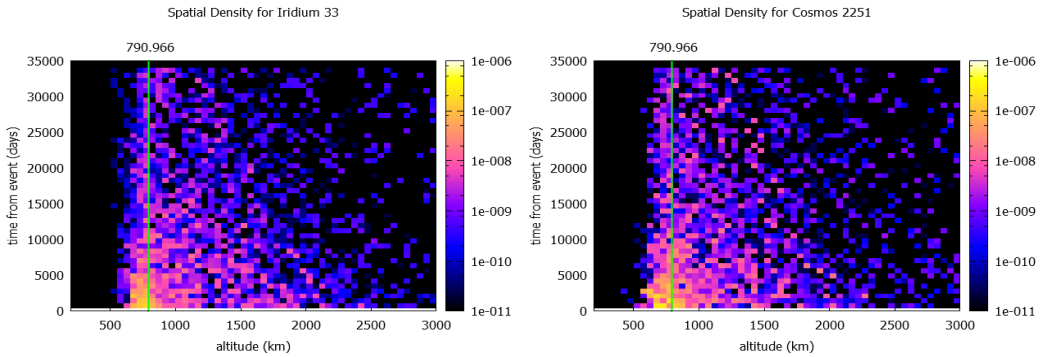

Figure 8: Spatial density for Cosmos-Iridium as a function of altitude over 100 years

The released collision pieces started to be catalogued by the JSpOC (Joint Space Operations Center) and added to the TLE catalogue starting with 18 February 2009. Catalogues with the fragments from that epoch can be retrieved from [4].

The identification of the fragmentation event was simulated with SOFT using as input a catalogue with fragments from TLE data of 19 February 2009. As background catalogue, we used another TLE catalogue that contained the space population as of 09 February 2009.

Figure 9 9 shows the backward propagation of the clouds until the time of event was identified. According to SOFT the fragmentation happened on 2009-02-10 16:55:40.038 for Cosmos 2251 and on 2009-02-10 16:47:30.038 for Iridium 33. The difference between the two results could be explain by different accuracy of the clouds observation and also because TLEs do not provide information about mass and diameter and random values are associated to them for propagation.

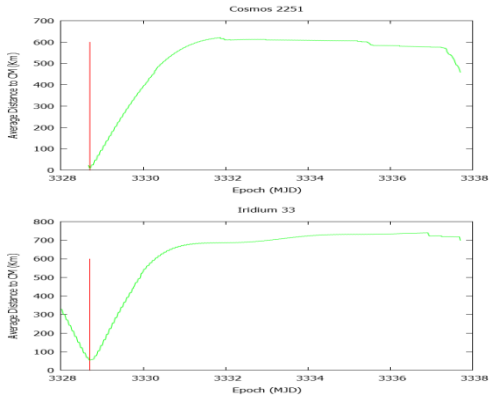

Figure 9: Backwards propagation of clouds Cosmos 2251 and Iridium 33

The tool correctly identified from the background catalogue the parents involved in the event. Tab. 5 lists the possible parents. For the second cloud two parents were selected as possible candidates, because the two objects have similar values for inclination and RAAN as the computed parent. The objects are listed ordered by their ID number. The object that has the values for inclination and RAAN closer than those of the computed parent is more likely to be the true parent.

The limitation of the space environment surveillance networks causes that the fragmentation clouds to be incomplete (not all fragments created in an event are detected) and inaccurate (the orbits of the fragments are known with a certain error). Fig. 10 shows the influence of inaccurate orbits over the identification of the fragmentation event. The position of the fragments was spoilt with different values of uncertainties in the along-track, cross-track and radial (ACR) directions. The magnitudes for the values of uncertainties used in each simulation are mentioned in the legend. In the cases in which that the position was spoilt with high level of uncertainties, 10 km along-track direction and 8 km along-track direction, the objects involved in the event were not identified from the background catalogue and although the computed time of event is close to real time, the error in terms of position of the event is considerable. For uncertainties smaller than 4 km along-track direction the results are similar to those without spoilt position.

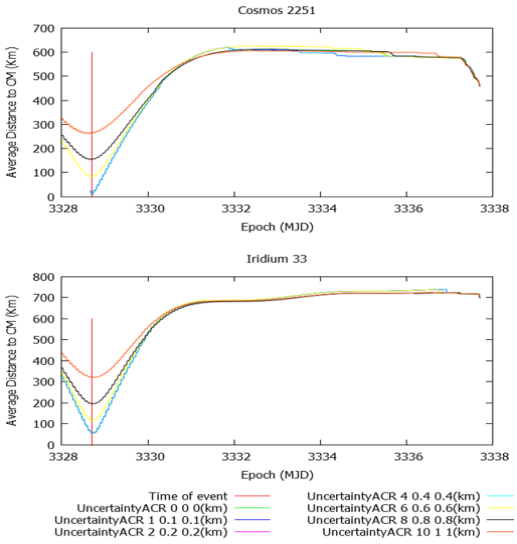

Figure 10: Identification of fragmentation event considering different values of uncertainties added to spoil the position of the fragments.

Table 5 : Objects identified by the SOFT tool as objects involved in the fragmentation (time in MJD2000)

	SMA [km]	Ecc	Inc [deg]	raan [deg]	Ident. time of event
Comp. Parent 1	7135.31	0.0048	74.05	17.12	3328.71
Orbital elements of candidate parents					
Cosmos 2251	7155.37	0.0012	74.04	17.16	3328.71
Comp. Parent 2	7089.52	0.007	86.42	121.11	3328.7
Orbital elements of candidate parents					
Cosmos 1470	6939.41	0.0015	82.55	119.19	3328.7
Iridium 33	7153.58	0.0014	86.45	121.20	3328.7

2.2 Explosion of Breeze-M R/B

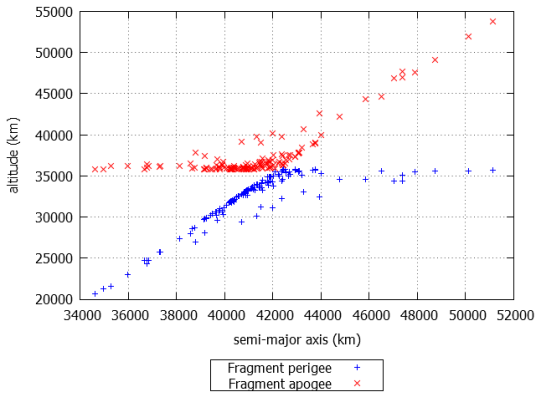

Figure 11: Gabbard diagrams for collision at the event epoch

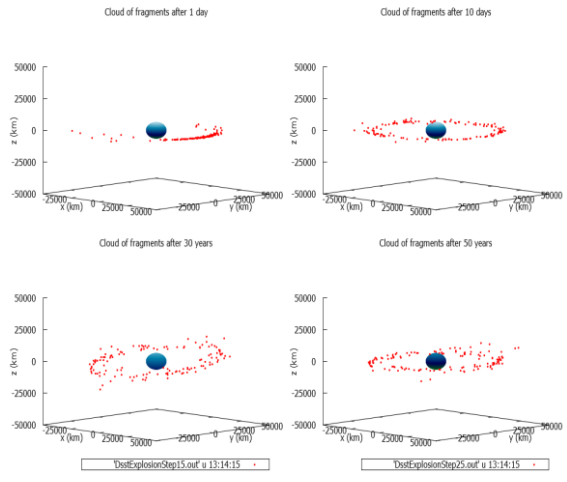

Figure 12: Evolution of the fragmentation clouds from Breeze-M R/B explosion. From left to right and from top to bottom, after : 1 day, 10 days, 30 years, 50 years.

For this case, the cloud of representative fragments larger than 10 cm is processed in IFEST for the computation of spatial density as a function of altitude and the cloud of representative fragments larger than 1 cm are used for the computation of spatial density as a function of longitude. Fig.11 reveals that, for this event, the Gabbard diagram shows the same characteristic X-shape. As illustrated in Figure *12* 12, the dispersion of the cloud is quite different and that is because the perturbations affect the cloud in a different way. The fragments do not disperse in latitude; the cloud plane remains almost intact, excepting a secular change in inclination produced by third-body perturbation.

Fig. 13 represents the spatial density as a function of longitude within a spherical shell defined between 35000 km and 36000 km. This plot shows the effect of resonant perturbations due to J22. The explosion occurs at longitude of -61.94° (61.94West). There are visible some curvilinear traces starting -61.94°, which characterise the part of the fragments that are oscillating around the stable point located at -105°. This effect is called libration. Fragments with higher delta-velocities avoid being captured by this stable point and circulate around the GEO ring. These plots also illustrate some linear traces that represent those high velocity fragments.

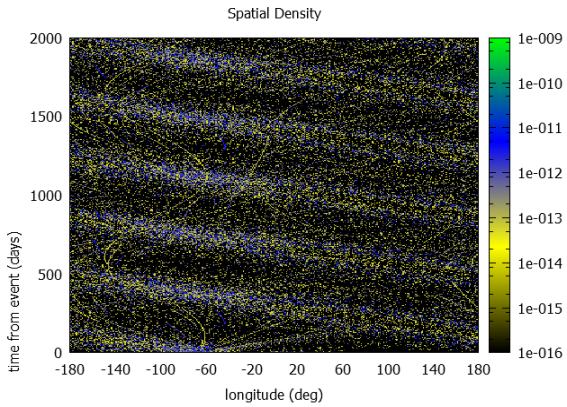

Figure 13: Spatial density as a function of longitude over 2000 days

Another typical secular trend is produced by third-body perturbations. It consists in the variation of inclination up to ±15° with a period of approximately 30 years. Fig. 14 shows this effect for all the propagated fragments.

The plots representing the spatial density (Fig. 15 Figure 15and Fig. 16) computed in IFEST show that almost all fragments stay close to the geosynchronous ring, although the parent object was not orbiting in a pure GEO orbit. These fragments pose a threat to the GEO protected region. Fig. 15 (left plot) also indicates the percent increment that this fragmentation event produces in the background spatial density provided by MASTER in the proximity of the GEO altitude, together with the GEO altitude (35786 km).

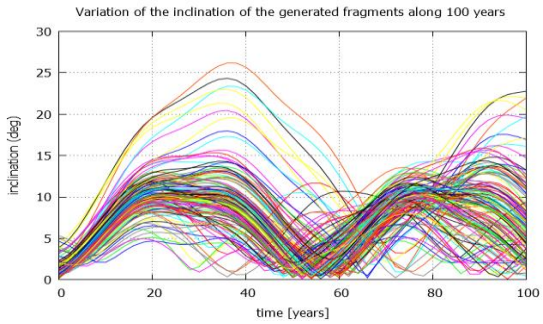

Figure 14: Variation of inclination for the fragments obtained from the explosion

For the simulation of Breeze-M R/B explosion, the SOFT tool used as input the cloud of fragments obtained from FREG. The fragments inside the cloud have the length greater than 1 cm. As background catalogue was used a TLE catalogue that contained the space population of 19 January 2016.

The cloud obtain by means of FREG tool is complete and the state vectors of the fragments are accurate. The identification of the fragmentation event is precise.

Figure *17* 17 shows the exact determination of time of event and position of the event. The drop-down right after the propagation started is caused by the elimination of a number of fragments, considered foreign object.

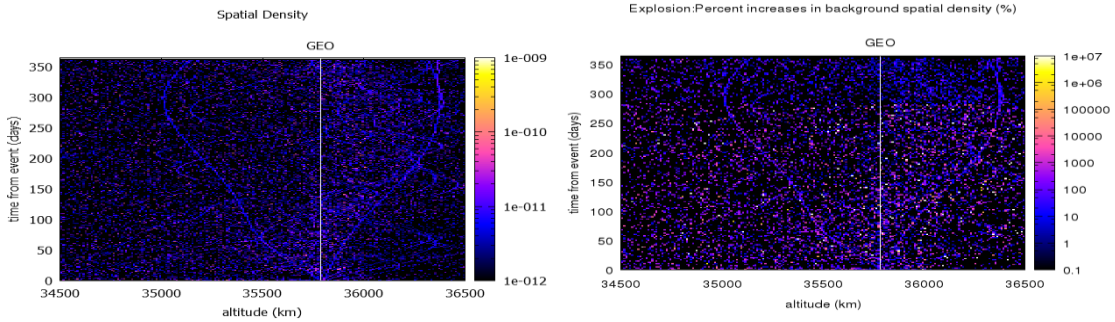

Figure 15: Spatial density and percent increases in background spatial density in the proximity of GEO altitude for Breeze-M R/B

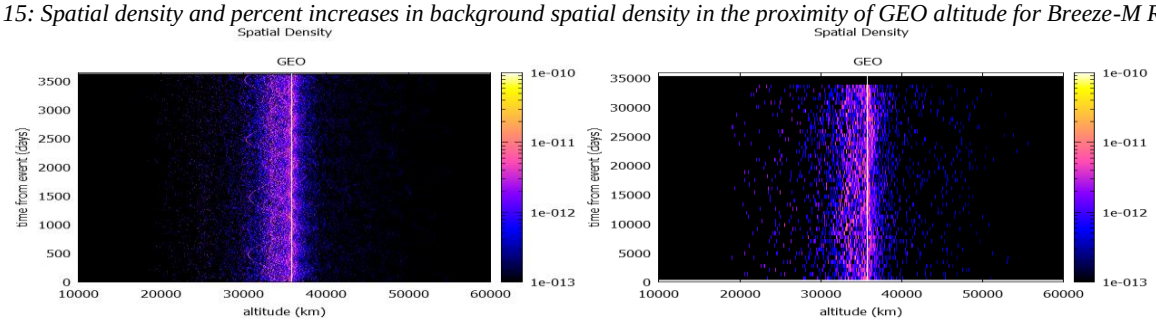

Figure 16: Spatial Density over 10 (left) and 100 years (right) for Breeze-M R/B

The possible parents are listed in Tab. 6. The objects are listed ordered by their ID number. The object that has the values for inclination, radius of perigee and apogee closer than those of the computed parent is more likely to be the true parent.

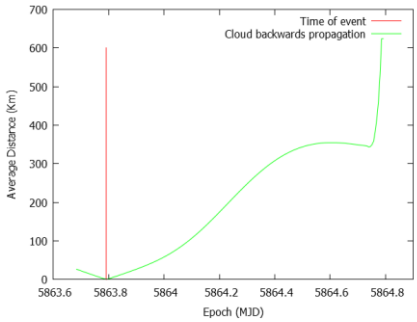

Figure 17: Backwards propagation of the fragmentation cloud

Table 6: Objects identified by the SOFT tool as possible parents (time in MJD2000)

	SMA [km]	**Ecc**	**Inc [deg]**	**Raan [deg]**	**Ident. Time of event**
Computed Parent	41064.59	0.0294	0.25	109.28	5863.79
Orbital elements of candidate parents					
SL-12 R/B(2)	41929.15	0.0021	14.51	357.27	5863.79
Breeze-M R/B	40979.09	0.0302	0.26	111.11	5863.79

In a real situation, a small number of fragments would be observed and the state vector of these fragments would not be so accurate. Fig. 18 represents the influence of inaccurate state vector over the identification of the fragmentation event. Like in the previous simulation the position of the fragments was

spoilt with different values of uncertainties in the ACR directions. The magnitudes for the values of uncertainties used in each simulation are mentioned in the legend. In all the simulated cases, the true parent was correctly identified from the background catalogue, although the error in terms of determining the position of the event is significant. In Fig. 19*Figure 19*, various simulation cases, using a different number of objects inside the fragmentation cloud are presented. The clouds converge to the correct concentration point.

However, when objects greater than 1 m were used, the true parent was not identified from the background catalogue. For the cases with 200, 136 and 54 fragments only the correct parent was identified from the background catalogue. For these simulations no uncertainties were added to the position.

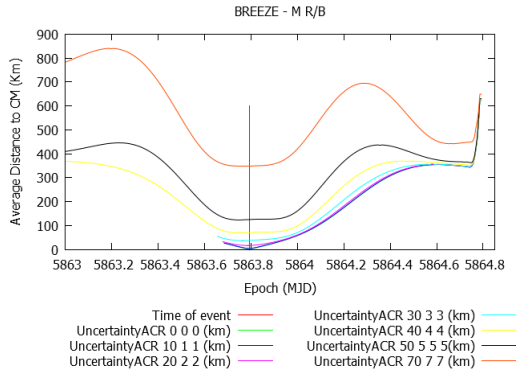

Figure 18: Identification of fragmentation event considering different values of uncertainties added to spoil the position of the fragments.

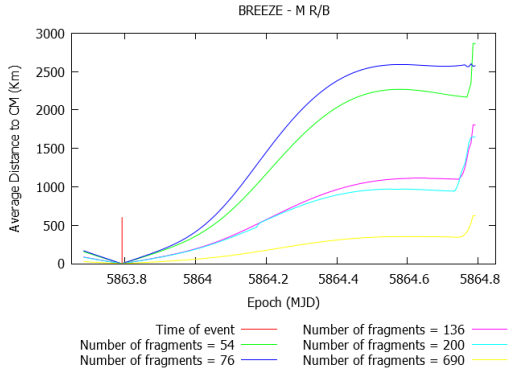

Figure 19: Identification of fragmentation event considering different number of fragments inside the cloud

3 CONCLUSIONS

The tools presented in this paper support the study of fragmentation events, either by simulating them or by using real orbital data obtained from a sensors network and also from TLE information. It is possible to study the long term effect of these events by means of the resulting spatial density, allowing comparison with the ESA MASTER tool. It is also possible to attempt to locate the position and orbit of the object(s) involved in the event in spite of having not complete clouds and poor accuracy. These tools can be used independently (in order to support studies such as the examples presented in this paper), or as part of a longer processing toolchain.

4 REFERENCES

1. D. A. Danielson C. P. Sagovac, B. Neta, L. W. Early, *Semianalytic Satellite Theory*, Mathematics Department, Naval Postgraduate School, Monterey, CA 93943

2. ESA, *Maintenance of the ESA MASTER Model*, Final Report, June 7, 2011

3. https://discosweb.esoc.esa.int/, January, 2016

4. www.space-track.org., March , 2016

5. https://www.orekit.org, March, 2016